THE JOURNAL OF BIOLOGICAL CHEMISTRY Vol. 275, No. 49, Issue of December 8, pp. 38605–38610, 2000
Printed in U.S.A.

Structure of the BH Domain from Graf and Its Implications for Rho GTPase Recognition*

Received for publication, August 18, 2000, and in revised form, September 9, 2000
Published, JBC Papers in Press, September 11, 2000, DOI 10.1074/jbc.M007574200

Kenton L. Longenecker‡, Baolin Zhang§, Urszula Derewenda‡, Peter J. Sheffield‡, Zbigniew Dauter¶‖, J. Thomas Parsons‡‡, Yi Zheng§, and Zygmunt S. Derewenda‡ ‡‡ §§

*From the ‡Department of Molecular Physiology and Biological Physics and the **Department of Microbiology, University of Virginia Health System, Charlottesville, Virginia 22908-0736, the §Department of Biochemistry, University of Tennessee, Memphis, Tennessee 38163, the ¶National Cancer Institute, Frederick, Maryland 21702, the ‖Brookhaven National Laboratory, Upton, New York 11973, and the ‡‡University of Virginia Cancer Center, Charlottesville, Virginia 22908*

Cellular signaling by small G-proteins is down-regulated by GTPase-activating proteins (GAPs), which increase the rate of GTP hydrolysis. The GTPase regulator associated with focal adhesion kinase (Graf) exhibits GAP activity toward the RhoA and Cdc42 GTPases, but is only weakly active toward the closely related Rac1. We determined the crystal structure of a 231-residue fragment of Graf (GrafGAP), a domain containing the GAP activity, at 2.4-Å resolution. The structure clarifies the boundaries of the functional domain and yields insight to the mechanism of substrate recognition. Modeling its interaction with substrate suggested that a favorable interaction with Glu-95 of Cdc42 (Glu-97 of RhoA) would be absent with the corresponding Ala-95 of Rac1. Indeed, GrafGAP activity is diminished ~40-fold toward a Cdc42 E95A mutant, whereas a ~10-fold increase is observed for a Rac1 A95E mutant. The GrafGAP epitope that apparently interacts with Glu-95(Glu-97) contains Asn-225, which was recently found mutated in some myeloid leukemia patients. We conclude that position 95 of the GTPase is an important determinant for GrafGAP specificity in cellular function and tumor suppression.

The superfamily of small molecular weight G-proteins contains a subfamily of Ras-homology (Rho)[1] proteins, which include RhoA, Cdc42, and Rac1 (1). Rho proteins regulate multiple cellular processes, including diverse aspects of cytoskeletal organization and gene expression (2). Improper mediation of these functions by Rho proteins is thought to play a fundamental role in human diseases such as hypertension and cancer (3, 4). Like other family members, these proteins act as molecular switches by cycling between GDP- and GTP-bound states, in which the GTP-bound form activates intracellular signaling pathways, whereas the GDP-bound form is biologically inactive. Progression through the GDP/GTP cycle is promoted by guanine nucleotide exchange factors, which stabilize the nucleotide-free form (5), and GAPs, which accelerate the enzymatic hydrolysis of the bound GTP to GDP (6).

GAPs for GTPases of the Rho family (RhoGAPs) contain a ~200-residue fragment known as the BH domain that is responsible for the GAP activity (7). The general mechanism by which GAPs function can be inferred from structures of p50RhoGAP in complex with either RhoA (8, 9) or Cdc42 (10). The GAP donates the side chain of an arginine to the active site of the GTPase and stabilizes Gln-61 (Gln-63 for RhoA), orienting a water molecule properly for hydrolysis of the γ-phosphate (6). Although this "arginine-finger" is necessary, other interactions are also important for GAP activity. For example, the BH domain of p85PI3-kinase ($BH_{PI3\text{-}K}$) contains the conserved arginine and binds Rho GTPases, but it does not possess GAP activity (7, 11). Although the mechanism by which GAPs down-regulate Rho GTPases is of fundamental interest, the means of substrate recognition is especially important. Cellular regulation requires selective activation of numerous pathways, and accordingly, wide substrate specificity is observed among RhoGAPs. Determining how different Rho GTPases are recognized by various GAPs is crucial to our understanding of regulatory cascades, but the structural determinants defining these preferences are not yet known (12).

Graf is a multi-domain protein that binds focal adhesion kinase and influences cytoskeletal changes mediated by Rho proteins (13, 14). Recently, the human *Graf* gene was found to be mutated in patients with myelodysplastic syndrome and acute myeloid leukemia (15). Graf contains a centrally located BH domain (GrafGAP), which displays a preference for Cdc42 and RhoA over Rac1 (13). We recently reported the crystallization of avian GrafGAP (16), and now we describe its structure and new biochemical data regarding its substrate specificity. With greater than 95% sequence identity to the human GrafGAP, this structure provides a molecular basis for understanding the mechanism of tumor suppression by Graf. Because GrafGAP exhibits more stringent substrate preferences than the p50RhoGAP, we are able to identify a structural basis of substrate discrimination by GrafGAP, yielding an important addition to structures of p50RhoGAP and $BH_{PI3\text{-}K}$ for understanding molecular specificity in this family of signal transduction proteins. Moreover, this work sheds light on other RhoGAP proteins, including a closely related homolog of Graf, oligophrenin-1, a protein involved in X-linked mental retardation (17).

EXPERIMENTAL PROCEDURES

Sample Preparation—The recombinant GrafGAP protein was expressed in *Escherichia coli*, purified, and crystallized as described pre-

* This project was funded by National Institutes of Health Grants HL48807 (to Z. S. D.) and GM60523 (to Y. Z.). The costs of publication of this article were defrayed in part by the payment of page charges. This article must therefore be hereby marked "*advertisement*" in accordance with 18 U.S.C. Section 1734 solely to indicate this fact.

The atomic coordinates and structure factors (code 1F7C) have been deposited in the Protein Data Bank, Research Collaboratory for Structural Bioinformatics, Rutgers University, New Brunswick, NJ (http://www.rcsb.org/).

§§ To whom correspondence should be addressed: Tel.: 804-243-6842; Fax: 804-982-1616; E-mail: ZSD4N@virginia.edu.

[1] The abbreviations used are: Rho, Ras-homology; GAP, GTPase-activating protein; PCMBS, *p*-chloromercuribenzene sulfonate; MES6, 2-amino-6-mercapto-7-methylpurine ribonucleoside; RMSD, root mean square deviation.

TABLE I

X-ray diffraction data and refinement statistics

$R_{sym} = \Sigma|I - \langle I\rangle|/\Sigma I$, where I is the integrated intensity for a reflection. $R_{iso} = \Sigma|F_{PH} - F_p|/\Sigma F_p$, where F_{PH} and F_p are the scaled structure factor amplitudes of the derivative and native. Phasing power = $\langle F_H\rangle/\langle$lack of closure$\rangle$, where F_H is the heavy-atom structure factor. Figure of merit = $\langle\Sigma P(\alpha)e^{i\alpha}/\Sigma P(\alpha)\rangle$, where $P(\alpha)$ is the phase probability at the angle α. $R_{cryst} = \Sigma|F_P - F_C|/\Sigma F_p$, where F_P and F_C are the observed and calculated structure factor amplitudes. R_{free} is the same as R_{cryst}, but calculated on ~10% of the data excluded from refinement. Values in parenthesis are for the highest resolution shell.

	Native 1	PCMBS	Baker's reagent	Uranyl acetate	Native 2
Resolution, d_{min} (Å)	2.4	3.2	3.2	3.0	3.0
Observations	30,884	9153	12,787	12,349	31,953
Unique reflections	9,020	3,684	3,899	4,741	4,732
Completeness (%)	99 (98)	93 (94)	99 (99)	99 (100)	99 (100)
I/σ_I	11.4 (2.8)	11.0 (4.0)	11.9 (5.0)	12.2 (3.6)	13.4 (10)
R_{sym} (%)	7.7 (33)	7.7 (26)	7.0 (22)	7.4 (29)	8.9 (28)
R_{iso} (%)		14	18	21	
MIR phasing statistics					
Resolution range (Å)		15–3.3	15–3.5	15–4.0	
Number of sites		1	2	1	
Phasing power (acentric/centric)		1.48/1.22	0.91/0.85	0.54/0.41	
		Mean figure of merit = 0.45			
Refinement (2.0–2.4 Å)					
R_{cryst}/R_{free} (%)	20.5/25.2	Molecular replacement using main chain atoms of p50RhoGAP yielded a correlation coefficient of 59 and an R-factor of 50% with the Native 2 data between 15 and 4.0 Å.			
Nonhydrogen atoms	1496				
Solvent molecules	47				
RMSD ideal bond lengths (Å)	0.006				
RMSD ideal bond angles (°)	1.12				
Average B-factor (Å^2)	47				

viously (16). Briefly, a purified glutathione *S*-transferase fusion construct was cleaved with rTEV protease (Life Technologies), and the components were separated by Superdex 75-gel filtration chromatography. Purified protein at 8 mg/ml crystallized in 20–22% polyethylene glycol 6000, 100 mM HEPES, pH 7.0.

X-ray Data Collection—The x-ray diffraction data were generated using Cu Kα radiation and collected at room temperature with a RAXIS IV detector (Rigaku). The data exhibited the symmetry of space group $P3_121$ or $P3_221$, and the cell dimensions of a = 65.0 Å, c = 91.6 Å suggested there was one molecule per asymmetric unit. Because the initial data failed to yield a convincing molecular replacement solution, potential heavy atom derivatives were screened. Three useful derivatives were prepared by soaking crystals individually in stabilizing medium (25% polyethylene glycol 6000, 100 mM HEPES, pH 7.0) with either 1 mM PCMBS or 1 mM Baker's dimercurial reagent for 1 week, or 2.5 mM uranyl acetate for 24 h. Additionally, data from a native crystal (Native 1) was combined with data collected from a second native crystal using a DIP2000 detector (MacScience), yielding a data set (Native 2) more complete and redundant in the lower resolution ranges. All data were scaled and reduced using the HKL suite (18), and intensities were converted to structure factor magnitudes using TRUNCATE (19).

Structure Determination—The Hg substructure for the PCMBS derivative was determined by SHELXS-97 (20) using isomorphous differences with native data, and the other derivatives were solved by difference Fourier techniques. Heavy atom parameters were refined using MLPHARE (19), and the resulting phases to 3.3 Å were subjected to density modification and phase extension to 3.0 Å with DM (19). Inspection of electron density maps from parallel calculations revealed the correct space group as $P3_121$ rather than its polar mate. A molecular replacement solution consistent with the experimental maps was found using the main chain atoms of the p50RhoGAP structure (Protein Data Bank code: 1RGP, residues 63–232) and the Native 2 data with the program AMORE (19). All solutions from the rotation search (15–5.0 Å) were subjected to a translational search (15–5.0 Å) and, subsequently, to rigid body refinement (15–4.0 Å), yielding a correlation coefficient of 58.6 and R-factor of 50.0%, whereas the top values for a wrong solution were 49.9 and 54.0%, respectively. Calculations with $BH_{PI3\text{-}K}$ (PDB code: 1PBW, residues A129-A298) yielded similar results, but with a weaker signal-to-noise ratio. A model for refinement was constructed by trimming portions of the molecular replacement solution and adding side chains for residues that exhibited electron density in the experimentally phased map. This initial model constituted 60% of the atoms in the final refined structure. The model was refined in CNS (21) using torsion-angle annealing with a maximum likelihood target toward the structure factor magnitudes of Native 1 data and the phase information encoded in the HL-coefficients output from MLPHARE. Electron density maps were calculated by combining experimental phases and sigmaa-weighted phases from the model, and the program O (22) was used for model building. Solvent molecules were automatically identified from difference Fourier maps and added manually. The model was evaluated using the programs OOPS (23) and PROCHECK (24) during iterative cycles of rebuilding and refinement.

GTPase Activity Measurements—Recombinant proteins were similarly expressed as glutathione *S*-transferase fusions in *E. coli* and prepared by established methods (25). The Rac1 A95E mutant was made using the QuikChange site-directed mutagenesis kit (Stratagene), by modifying a pGEX-4T vector encoding Rac1 and confirming the mutation by DNA sequencing. Constructs for other proteins were produced in former studies. The intrinsic and GAP-stimulated GTPase activities were measured using the nitrocellulose filter binding assay as described previously (12). The GTPases were preloaded with [γ-^{32}P]GTP and incubated with reaction buffer in the presence or absence of GrafGAP. Reactions were terminated after 1 min by filtration through nitrocellulose filters, and the retentions of G-protein-bound radioactivity were quantified using a scintillation counter. The kinetics of the GTPase enhancement by GrafGAP were also performed and analyzed as previously published (12). Briefly, the γP_i release from GTP-loaded GTPases was measured using the continuous spectroscopic assay of a coupled MESG/phosphorylase system. The absorptions at 360 nm of the P_i-coupling reactions were monitored during the time course in a buffer (20 mM Tris-HCl, pH 7.6, 0.1 mM EDTA, 200 μM GTP, and 0.2 mM MESG) with 10 units of purine nucleoside phosphorylase at 20 °C, which provides a condition for the G-protein to undergo multiple turnover. At time zero, a final concentration of 5 mM $MgCl_2$ was added to initiate the single turnover reactions. The initial rates of GTP-hydrolysis monitored by γP_i release were determined in the presence of a constant amount of GrafGAP and increasing concentrations of GTP-loaded enzymes. GrafGAP concentrations of 2, 10, and 100 nM were used for Cdc42, RhoA, and Rac1, respectively, and 50 nM was used for Cdc42 E95A and Rac1 A95E, all of which are within the linear ranges of the absorbance measurements. The GAP-catalyzed GTP hydrolysis rates were fitted by nonlinear regression into the modified Michaelis-Menten equation to yield the K_m and V_{max} values of the reactions (12). The k_{cat} values were calculated as V_{max}/[GrafGAP], allowing the overall catalytic efficiencies k_{cat}/K_m to be derived.

RESULTS AND DISCUSSION

Structure of GrafGAP—The structure of avian GrafGAP was determined by x-ray crystallography, using a combination of molecular replacement and heavy atom isomorphous replace-

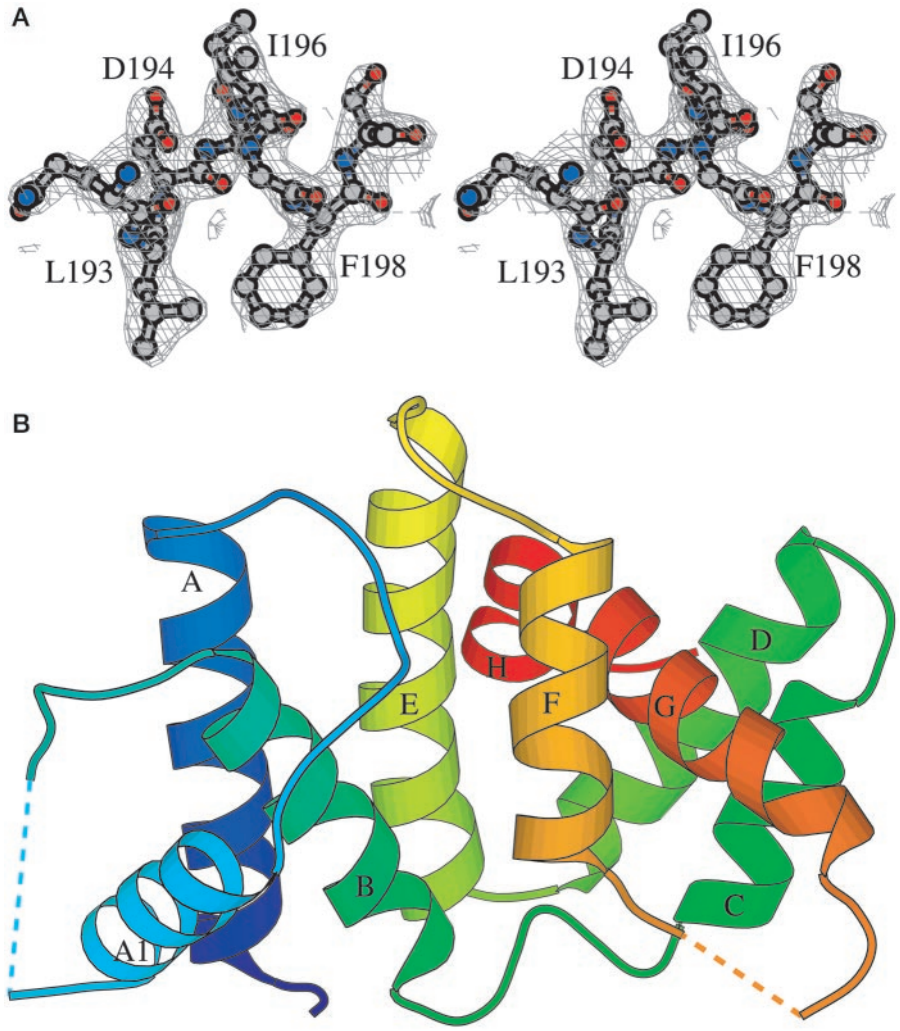

FIG. 1. **Structure of GrafGAP.** *A*, this stereo view of the final $2F_o - F_c$ map, contoured at 1.0 σ, shows the electron density of Leu-193, which stabilizes the N-terminal boundary of the BH domain. *B*, the ribbon drawing colored from the N terminus (*blue*) to C terminus (*red*) illustrates the overall fold of GrafGAP. Secondary elements are labeled as for structures of $BH_{PI3\text{-}K}$ and p50RhoGAP (7, 26). This figure was prepared with BOBSCRIPT (27).

ment techniques, and was refined to a resolution of 2.4 Å (Table I). GrafGAP contains a bundle of nine α helices packed together in an anti-parallel arrangement (Fig. 1), assuming a fold similar to that of p50RhoGAP (26) and $BH_{PI3\text{-}K}$ (7). The overall similarity of these structures is implied by the successful molecular replacement solution used in the structure determination. Upon alignment of a core portion of the models containing the five central helices, the root mean square deviation of the displacement for 92 α-carbon atoms of GrafGAP compared with p50RhoGAP and BH_{PI3K} is 0.88 Å and 1.03 Å, respectively, and slight displacements of the peripheral loops and helices are apparent (Fig. 2). The common overall fold was anticipated by sequence alignment (Fig. 2). GrafGAP shares approximately 25% identity to the sequences of p50RhoGAP and $BH_{PI3\text{-}K}$ over the common structural domain. Slightly higher sequence identity is shared with several other GAPs (*e.g.* 37% with β-chimaerin (13)), but the closest similarity is found with oligophrenin-1, sharing 55% identity with GrafGAP over the BH domain (17).

The recombinant GrafGAP construct (residues 161–391) includes about 20 residues that are conserved between GrafGAP and oligophrenin-1 at the N terminus of the BH domain. The corresponding fragment in p50RhoGAP is ordered and has been considered an integral part of the BH domain. However, the first 30 residues are not evident in the electron density map, and consequently we believe that they are not ordered; the same is true of the final 10 residues. Thus, the ordered portion of the structure allows for a precise definition of the boundaries of the BH domain, comprising residues 191–381 (numbers based on full sequence of Graf). Notably, a GrafGAP construct truncated at these boundaries displays GAP activity unchanged from that exhibited by the crystallized protein (data not shown), further underscoring the compact architecture of this BH domain. Sequence similarity would suggest similar boundaries for the corresponding regions in oligophrenin-1 and closely related RhoGAPs.

The ends of the BH domain in Graf are stabilized by hydrophobic interactions that differ in detail to those observed in other BH domain structures. Specifically, the N-terminal boundary is stabilized by the packing of Leu-193 between helices A, B, and E. This leucine adopts a similar arrangement as is found for Leu-49 in p50RhoGAP and Leu-118 in BH_{PI3K} (numbering as in crystal structures (7, 26)). However, the leucines in the latter structures belong to a helix preceding helix A, whereas the path of the main chain following Leu-193 of Graf leads directly into helix A, two residues away (Fig. 1). The C terminus of the BH domain is similarly stabilized by hydrophobic interactions, whereby Ile-375 and Phe-376 firmly wedge helix H between helices D and E. These residues form interactions similar to those found for Leu-233 and Phe-234 in p50RhoGAP, but the corresponding local structure in $BH_{PI3\text{-}K}$ is stabilized differently.

Two other regions with particular flexibility, showing no ordered structure in electron density maps, are the short loops located between helices A1 and B, and between helices F and G (Fig. 1). No known function can be assigned to the first disordered loop, but the second loop would be expected to become

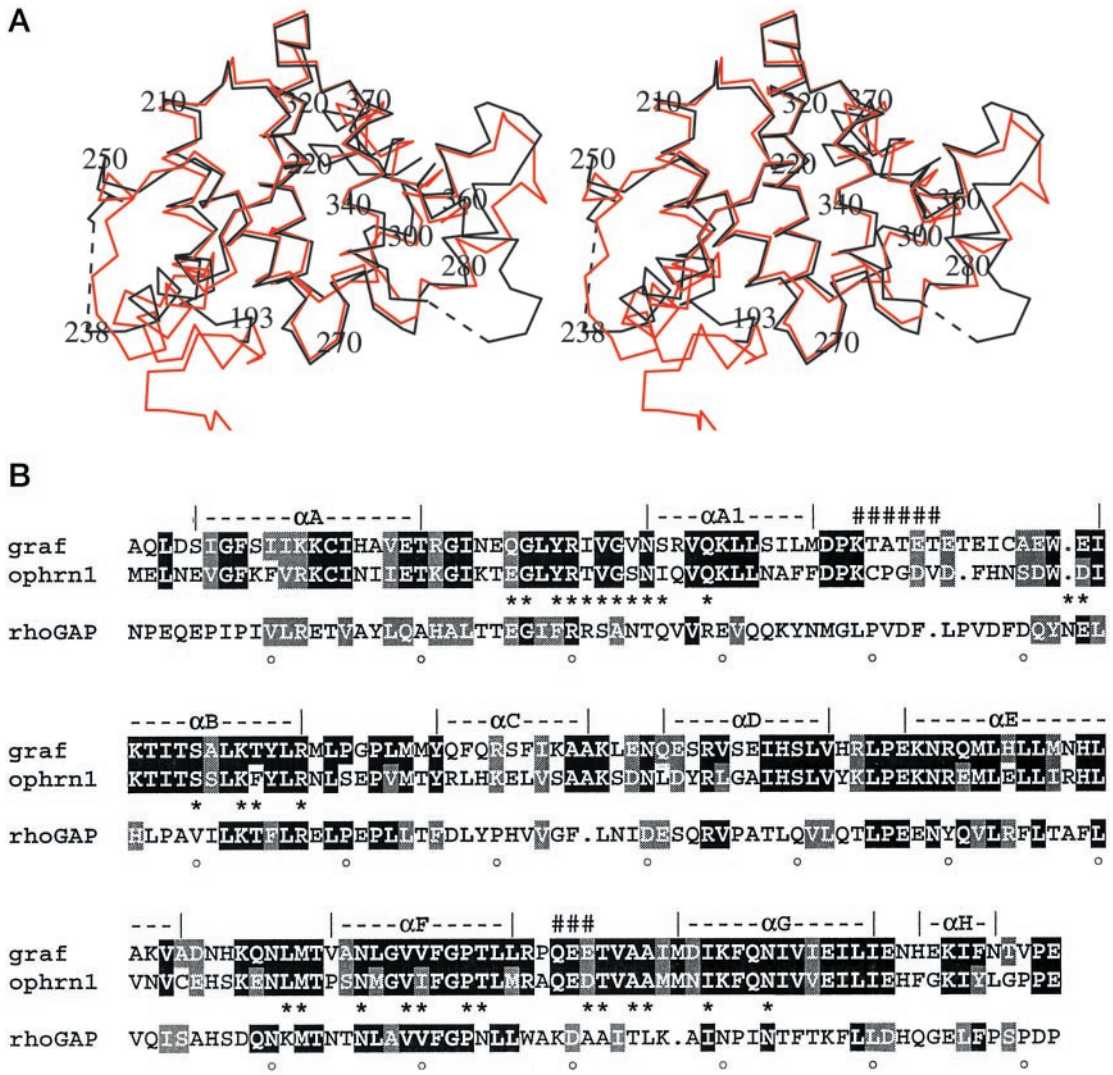

FIG. 2. **Comparison of GrafGAP with other RhoGAPs.** *A*, the α-carbon trace of GrafGAP (*black*) is shown in stereo together with the aligned trace of p50RhoGAP (*red*) in the same orientation as Fig. 1*B*. *B*, sequence alignment shows the amino acid similarity between the BH domains from Graf (residues 191–381), oligophrenin-1 (residues 380–569), and p50RhoGAP (residues 56–239, numbering as PDB code 1RGP (26)). Residues conserved with GrafGAP are *shaded*, and secondary structural elements are identified. Disordered residues are noted (#), and residues of p50RhoGAP that are within 5 Å of RhoA in the transition state complex (9) are labeled (*).

ordered upon binding a G-protein, because the corresponding region in p50RhoGAP is observed to form part of the structurally ordered interface in a complex with RhoA or Cdc42 (9, 10). Incidentally, this region in the structure of free p50RhoGAP is also disordered (26).

GTPase Activation and Substrate specificity—Graf was previously shown to have RhoGAP activity, displaying a preference for Cdc42 and RhoA over Rac1 (13). This preference is confirmed and quantified by measurements of the kinetic parameters for the activity of GrafGAP (Table II). With micromolar values of K_m, the overall catalytic efficiency k_{cat}/K_m of GrafGAP is ~10-fold higher for Cdc42 than for RhoA, and about 1000-fold greater than for Rac1. Values obtained from these experiments compare well with those for p50RhoGAP in similar experiments toward Cdc42 and RhoA (12). However, the lower efficiency that GrafGAP exhibits toward Rac1 is reflected in both a higher K_m and lower k_{cat}.

To model the structural interactions between GrafGAP and substrate, the structure of GrafGAP was docked as a rigid body into a position occupied by p50RhoGAP bound to RhoA or Cdc42 in structures of the transition state complexes (Fig. 3). Many of the residues of p50RhoGAP at the interface with the GTPase are conserved between both GrafGAP and oligophrenin-1 (Fig. 2*B*). The conserved "arginine-finger" in GrafGAP, Arg-220, is located close to the active site and would need to reorient slightly to attain a transition state configuration, a change also observed between the free and bound structures of p50RhoGAP (9). The proximity of helix A1 of GrafGAP to helix α3 of the GTPase is also evident, and we noted the possibility for substrate discrimination by GrafGAP based on the type of amino acid found at position 95 of the GTPase (Glu-97 in RhoA). A glutamate residue conserved at this position in Cdc42 and RhoA appears to interact with the N terminus of helix A1 in GrafGAP. Specifically, an alternate side-chain rotamer places the negative charge of the glutamate close to two uncapped main-chain amides belonging to Asn-225 and Ser-226 of GrafGAP (Fig. 3*B*). Furthermore, the side chain of Asn-225 would also likely interact with the side chain of Glu-95(Glu-97) of the GTPase. These favorable interactions would be lost with Rac1, which has an alanine at the corresponding position (Fig. 3*C*).

The basis for the substrate specificity suggested by this modeling was tested by measuring the activity of GrafGAP toward the single-site mutants Cdc42 E95A and Rac1 A95E. Retention of γ-^{32}P-labeled nucleotide by the GTPase in the presence of GrafGAP was assessed using a nitrocellulose filter binding

TABLE II
Kinetic parameters GrafGAP exhibits toward Rho GTPases

Rho GTPase	K_m	V_{max}	k_{cat}	k_{cat}/K_m
	μM	$\mu M/min$	min^{-1}	$\mu M^{-1}\ min^{-1}$
Cdc42	3.06 ± 0.16	2.32 ± 0.03	1160 ± 15	379.1
RhoA	3.99 ± 0.30	1.56 ± 0.09	156 ± 9	39.1
Rac1	11.8 ± 0.8	0.51 ± 0.05	5.1 ± 0.5	0.43
Cdc42 E95A	10.3 ± 1.9	4.46 ± 0.38	83.6 ± 7.6	9.1
Rac1 A95E	5.56 ± 0.79	1.18 ± 0.06	23.6 ± 1.2	4.2

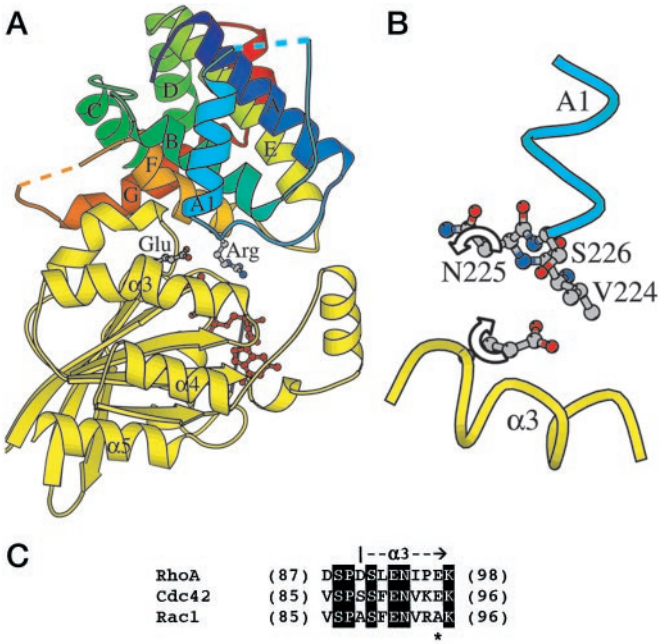

FIG. 3. **Modeling the interaction of GrafGAP with substrate.** *A*, view of GrafGAP docked as a rigid body into the position of p50RhoGAP bound to RhoA in the transition state complex. GrafGAP is colored as in Fig. 1*B*, and the GTPase is colored *yellow*. The conserved "arginine-finger" in GrafGAP, and the glutamate residue in the GTPase that is important for substrate selectivity are shown together with the position of the nucleotide. *B*, the molecular basis of GrafGAP specificity as proposed by modeling is shown, suggesting that Glu-95 of Cdc42 (Glu-97 of RhoA) adopts an alternate rotomer, which interacts with the N terminus of helix A1 (*blue*) from GrafGAP. *C*, amino acid sequence alignment of RhoA, Cdc42, and Rac1 is shown for a region that forms part of the interface upon binding the GAP. Conserved residues are *shaded*, and Glu95 (Glu-97) of the GTPase is noted by an *asterisk*.

assay (12). GrafGAP activity toward Cdc42 E95A was reduced in comparison with wild-type, whereas GrafGAP activity toward Rac1 A95E was correspondingly increased (Fig. 4). To quantify these changes more carefully, we measured the kinetic parameters for these mutants. The overall catalytic efficiency k_{cat}/K_m for the Cdc42 E95A mutant was reduced ~40-fold compared with wild-type, whereas that for the Rac1 A95E mutant was increased ~10-fold above wild-type Rac1 (Table II). The dramatic effect of this single mutation is apparently due to direct changes in affinity for GrafGAP rather than secondary effects on GTPase activity, for the intrinsic GTPase activity of the mutants remains unchanged. Changes in K_m observed between mutant and wild-type enzymes correspondingly indicate the glutamate side chain promotes interaction with GrafGAP. We conclude that the residue at position 95 of the GTPase forms an important determinant of substrate discrimination for GrafGAP.

The importance of the interaction between helix A1 of GrafGAP and helix α3 of the GTPase is consistent with the general nature of the movement from the ground state (8) to the transition state (9) observed in GTPase complexes with p50RhoGAP (6). A shift in the position of p50RhoGAP is observed, largely characterized as a 20° rigid-body rotation about the GTPase, resulting in helix A1 of p50RhoGAP dramatically moving 6 Å toward the helix α3 of the GTPase. In the transition state, Asn-94 and Glu-97 on helix α3 of RhoA form hydrogen bonds with p50RhoGAP, pulling the helix A1 loop close to the GTPase. Correspondingly, in the transition state complex with Cdc42, Asn-92 interacts with p50RhoGAP, but in this case Glu-95 of Cdc42 does not form a hydrogen bond across the interface. Although the interface includes interactions between helix A1 of p50RhoGAP and the helix α3 of the GTPase, the activity p50RhoGAP exhibits toward all Rho family GTPases suggests interaction(s) with residue 95 of the GTPase is relatively less important for p50RhoGAP activity than for GrafGAP.

The configuration of the main chain leading into helix A1 in GrafGAP is similar to p50RhoGAP (Fig. 2) but is in striking contrast to that observed in the structure of $BH_{PI3\text{-}K}$. Upon alignment with transition state structures, helix A1 of $BH_{PI3\text{-}K}$ is not capable of similar interactions with the GTPase. The reason $BH_{PI3\text{-}K}$ lacks GAP activity has been unclear, but was tentatively attributed to the lack of a conserved asparagine residue corresponding to Asn-194 in p50RhoGAP (6, 26). In addition, we suggest that the loop preceding helix A1 simply does not allow the close apposition to the GTPase necessary for properly orienting the "arginine-finger" into the active site. The specific determinants important for binding and GAP activation, however, are expected to vary among GAPs. For example, kinetic experiments comparing the GAP activity of p190GAP and p50RhoGAP toward RhoA show a much greater salt dependence for the former than the latter, suggesting the greater importance of charged interactions for p190GAP than for p50RhoGAP (12). Despite the variation among the family of GAPs, the high degree of amino acid conservation between GrafGAP and oligophrenin-1 would suggest similar interactions with the GTPase. We surmise that the residue at position 95 of the GTPase might also partially explain an apparent preference of oligophrenin-1 for Cdc42 and RhoA over Rac1 (17).

Interestingly, new data support the role of tumor suppressor for Graf. In some myeloid leukemia patients, the *Graf* gene is fused to the *mixed-lineage leukemia* gene, losing the GAP domain (15). The residual allele, potentially sufficient to suppress the syndrome, was found to contain mutations, one of which affects Asn-225 (15). This residue, along with all the other residues that would interface with the GTPase, is conserved between the avian and human isoforms of GrafGAP. These observations reinforce our conclusion that the Asn-225 containing epitope of GrafGAP is critical for its biological function, which is proper selection of the target GTPase.

The overall preference GrafGAP exhibits *in vitro* differs from that observed recently *in vivo*. Although our data would suggest that Cdc42 is the preferred substrate of Graf, the cytoskeletal changes induced by Graf *in vivo* are processes thought to be dependent specifically upon RhoA and not Cdc42 (14). This would suggest Graf has some other means of distinguishing G-proteins *in vivo* in addition to the specificity determinant we identify here. The present study addresses the specificity in-

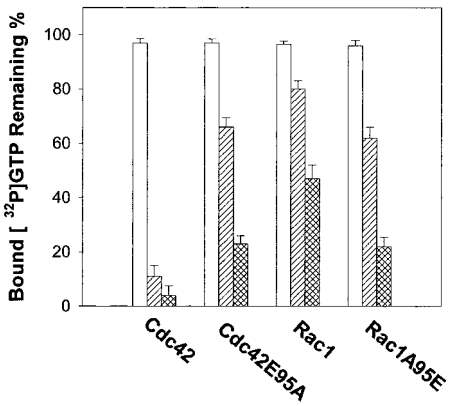

FIG. 4. **Amino acid type at position 95 of Cdc42 or Rac1 is an important determinant for GrafGAP activity.** The relative sensitivity of 5 μM Rho GTPases to activation were measured in the absence (*open bars*) or presence of 50 nM GrafGAP (*dashed bars*) or 200 nM GrafGAP (*double-dashed bars*) by the nitrocellulose filter binding assay.

herent to the GrafGAP domain and does not account for any additional substrate selectivity based on other factors, such as subcellular localization or additional interactions occurring outside the BH domain. These results reveal novel structural features for the regulation of Rho GTPases by Graf and yield insight to the molecular properties of oligophrenin-1 and other related GAPs.

REFERENCES

1. Mackay, D. J., and Hall, A. (1998) *J. Biol. Chem.* **273,** 20685–20688
2. Kaibuchi, K., Kuroda, S., and Amano, M. (1999) *Annu. Rev. Biochem.* **68,** 459–486
3. Uehata, M., Ishizaki, T., Satoh, H., Ono, T., Kawahara, T., Morishita, T., Tamakawa, H., Yamagami, K., Inui, J., Maekawa, M., and Narumiya, S. (1997) *Nature* **389,** 990–994
4. Zohn, I. M., Campbell, S. L., Khosravi-Far, R., Rossman, K. L., and Der, C. J. (1998) *Oncogene* **17,** 1415–1438
5. Cherfils, J., and Chardin, P. (1999) *Trends Biochem. Sci.* **24,** 306–311
6. Gamblin, S. J., and Smerdon, S. J. (1998) *Curr. Opin. Struct. Biol.* **8,** 195–201
7. Musacchio, A., Cantley, L. C., and Harrison, S. C. (1996) *Proc. Natl. Acad. Sci. U. S. A.* **93,** 14373–14378
8. Rittinger, K., Walker, P. A., Eccleston, J. F., Nurmahomed, K., Owen, D., Laue, E., Gamblin, S. J., and Smerdon, S. J. (1997) *Nature* **388,** 693–697
9. Rittinger, K., Walker, P. A., Eccleston, J. F., Smerdon, S. J., and Gamblin, S. J. (1997) *Nature* **389,** 758–762
10. Nassar, N., Hoffman, G. R., Manor, D., Clardy, J. C., and Cerione, R. A. (1998) *Nat. Struct. Biol.* **5,** 1047–1052
11. Zheng, Y., Bagrodia, S., and Cerione, R. A. (1994) *J. Biol. Chem.* **269,** 18727–18730
12. Zhang, B., and Zheng, Y. (1998) *Biochemistry* **37,** 5249–5257
13. Hildebrand, J. D., Taylor, J. M., and Parsons, J. T. (1996) *Mol. Cell. Biol.* **16,** 3169–3178
14. Taylor, J. M., Macklem, M. M., and Parsons, J. T. (1999) *J. Cell Sci.* **112,** 231–242
15. Borkhardt, A., Bojesen, S., Haas, O. A., Fuchs, U., Bartelheimer, D., Loncarevic, I. F., Bohle, R. M., Harbott, J., Repp, R., Jaeger, U., Viehmann, S., Henn, T., Korth, P., Scharr, D., and Lampert, F. (2000) *Proc. Natl. Acad. Sci. U. S. A.* **97,** 9168–9173
16. Sheffield, P. J., Derewenda, U., Taylor, J., Parsons, T. J., and Derewenda, Z. S. (1999) *Acta Crystallogr. Sect. D Biol. Crystallogr.* **55,** 356–359
17. Billuart, P., Bienvenu, T., Ronce, N., des Portes, V., Vinet, M. C., Zemni, R., Crollius, H. R., Carrie, A., Fauchereau, F., Cherry, M., Briault, S., Hamel, B., Fryns, J. P., Beldjord, C., Kahn, A., Moraine, C., and Chelly, J. (1998) *Nature* **392,** 923–926
18. Otwinowski, Z., and Minor, W. (1997) *Methods Enzymol.* **276,** 307–326
19. Collaborative Computational Project, Number 4 (1994) *Acta Crystallogr. Sect. D Biol. Crystallogr.* **50,** 760–763
20. Sheldrick, G. M. (1998) in *Direct Methods for Solving Macromolecular Structures*, (Fortier, S., ed) pp. 401–411, Kluwer Academic Publishers, Dordrecht
21. Brunger, A. T., Adams, P. D., Clore, G. M., DeLano, W. L., Gros, P., Grosse-Kunstleve, R. W., Jiang, J. S., Kuszewski, J., Nilges, M., Pannu, N. S., Read, R. J., Rice, L. M., Simonson, T., and Warren, G. L. (1998) *Acta Crystallogr. Sect. D Biol. Crystallogr.* **54,** 905–921
22. Jones, T. A., Zou, J. Y., Cowan, S. W., and Kjeldgaard, M. (1991) *Acta Crystallogr. Sect. A* **47,** 110–119
23. Kleywegt, G. J., and Jones, T. A. (1997) *Methods Enzymol.* **277,** 208–230
24. Laskowski, R. A., MacArthur, M. W., Moss, D. S., and Thornton, J. M. (1993) *J. Appl. Crystallogr.* **26,** 283–291
25. Li, R., Zhang, B., and Zheng, Y. (1997) *J. Biol. Chem.* **272,** 32830–32835
26. Barrett, T., Xiao, B., Dodson, E. J., Dodson, G., Ludbrook, S. B., Nurmahomed, K., Gamblin, S. J., Musacchio, A., Smerdon, S. J., and Eccleston, J. F. (1997) *Nature* **385,** 458–461
27. Esnouf, R. M. (1997) *J. Mol. Graph.* **15,** 132–143